Nano Research

ISSN 1998-0124 CN 11-5974/O4
https://doi.org/10.26599/NR.2026.94909011

Research Article

Multi-magnetic regulation of hollow CoNi microspheres via morphological evolution for ultrahigh electromagnetic wave absorption

Wenqi Song[1](✉), Chunyang Lan[1], Zhaona Du[1], Chenyu Wang[2], Panbo Liu[2](✉)

[1] Technological Institute of Materials & Energy Science (TIMES); Shaanxi Key Laboratory of Liquid Crystal Polymer Intelligent Display; Key Laboratory of Liquid Crystal Polymers based Flexible Display Technology in National Petroleum and Chemical Industry; School of Materials and New Energy, Xijing University, Xi'an 710123, China

[2] School of Chemistry and Chemical Engineering, Northwestern Polytechnical University, Xi'an 710129, China

Nano Res., **Just Accepted Manuscript** • https://doi.org/10.26599/NR.2026.94909011

https://www.sciopen.com/journal/1998-0124 on Jul. 7, 2026

© The Authors(s)

Just Accepted

This is a "Just Accepted" manuscript, which has been examined by the peer-review process and has been accepted for publication. A "Just Accepted" manuscript is published online shortly after its acceptance,which is prior to technical editing and formatting and author proofing. Tsinghua University Press (TUP) provides "Just Accepted" as an optional and free service which allows authors to make their results available to the research community as soon as possible after acceptance. After a manuscript has been technically edited and formatted, and the page proofs have been corrected, it will be removed from the "Just Accepted" web site and published officially with volume and article number (e.g., *Nano Research*, **2025**, *18*, 94906990). Please note that technical editing may introduce minor changes to the manuscript text and/or graphics which may affect the content, and all legal disclaimers that apply to the journal pertain. In no event shall TUP be held responsible for errors or consequences arising from the use of any information contained in these "Just Accepted" manuscripts. To cite this anuscript please use its Digital Object Identifier (DOI®),which is identical for all formats of publication.

Just Accepted

Research Article

Multi-magnetic regulation of hollow CoNi microspheres via morphological evolution for ultrahigh electromagnetic wave absorption

Wenqi Song[1,*], Chunyang Lan[1], Zhaona Du[1], Chenyu Wang[2], Panbo Liu[2,*]

[1]Technological Institute of Materials & Energy Science (TIMES); Shaanxi Key Laboratory of Liquid Crystal Polymer Intelligent Display; Key Laboratory of Liquid Crystal Polymers based Flexible Display Technology in National Petroleum and Chemical Industry; School of Materials and New Energy, Xijing University, Xi'an 710123, China

[2]School of Chemistry and Chemical Engineering, Northwestern Polytechnical University, Xi'an 710129, China

*Address corresponding to Wenqi Song, songwenqi@xijing.edu.cn; Panbo Liu, liupanbo@nwpu.edu.cn.

Received: 28 May 2026; Revised: 6 July 2026; Accepted: 7 July 2026

Cite this article: *Nano Research*, 2026, 19, 94909011

https://doi.org/10.26599/NR.2026.94909011

Just Accepted

Abstract

Hollow cavity and multi-magnetic components are of great significance in adjusting impedance characteristics and realizing ultrahigh electromagnetic wave attenuation. Inspired by this thought, hollow CoNi microspheres are successfully fabricated by a sacrificial template strategy, in which the morphological evolution via the cation exchange reaction plays an indispensable role in regulating the multi-magnetic components. Results reveal that hollow cavity significantly balances the impedance matching and establishes more conductive networks for the enhancement of conduction loss, the cation exchange process promotes the morphological evolution from polyhedral structure to 2D nanosheets and the compositional regulation from single to multi-magnetic components, and the formation of multiple hetero-interfaces induces strong interfacial polarization. As expected, the as-synthesized hollow CoNi microspheres display ultrahigh electromagnetic wave absorption, the maximum reflection loss is up to -62.9 dB and the absorption bandwidth achieves 7.5 GHz with only 15 wt% filler loading. Moreover, the specific reflection loss and specific effective absorption bandwidth are higher than the vast majority of counterparts, demonstrating the potential practical applications in the field of electromagnetic stealth and protection.

Keywords: hollow cavity, multi-magnetic components, morphological evolution, interfacial polarization, electromagnetic wave absorption

Just Accepted

1. Introduction

In the frontier of electromagnetic (EM) stealth and defense technology, precise optimization of matching impedance and significant enhancement of EM wave attenuation are considered as the most urgent concerns in the development of promising EM wave absorbing materials [1,2]. For practical applications, ideal EM wave absorbing materials should simultaneously possess some basic features, such as low filler content, high absorption performance, and thin thickness [3-5]. In order to realize these characteristics, abundant researchers focus on adjusting the EM parameters and promoting the absorption capacity by constructing hierarchical or core-shell structures [6-9], integrating dielectric-magnetic compositions [10,11], regulating phase transition [12-14], introducing built-in electric field [15-18], et al. Up to now, although significant achievements have been realized by these aforementioned strategies, it still faces huge challenges to balance the relationship between the EM parameters and absorption attenuation to realize excellent EM wave absorption performance at low filler loading.

In recent decades, metal-organic-frameworks (MOFs) derivatives with tunable porous structure, multiple hetero-interfaces and electromagnetic synergy have received widespread attention in the field of EM wave absorbing materials [19-25]. In order to achieve satisfied EM wave absorption, high filler loading is often required because most of MOFs derivatives possess solid structure and only sufficient loadings can establish effective conductive paths to decrease the percolation threshold in

Just Accepted

molecular-scale [26,27]. Besides, the intrinsic advantage of ordered porous structure of MOFs is destroyed after the pyrolysis treatment, resulting in the formation of unpredictable porous structure. Hollow engineering can introduce large interior void to optimize impedance matching and enhance interfacial polarization, thereby realizing excellent EM wave absorption at low filler loading [28]. Compared with traditional pyrolysis process, the presence of sacrificial templates can inhibit the inward shrinkage of organic frameworks during the pyrolysis process and preserve the original structure. Moreover, the removal of the templates can form controllable interior void, which is the ideal strategy in constructing hollow cavity [29]. The first research of hollow MOFs derivatives is reported by Du, who produced hollow Co/C microspheres by using CTAB as the templates [30]. Benefiting from the cooperative advantages of boost dielectric loss and matched impedance, the synthesized hollow Co/C microstructures displayed strong reflection loss (-66.5 dB) with 30 wt% filler loading. However, the removal of CTAB is time consuming and using corrosive agents. Encouraged by the synthetic approaches, protecting-etching and ion exchange are considered as the straightforward strategies to construct hollow MOFs derivatives. Benefiting from the delicate control of hollow cavity and the controllable compatibility of multi-magnetic components, these obtained hollow derivatives could display ultrahigh EM wave absorption [31-33].

Herein, we have synthesized hollow CoNi microspheres with multi-magnetic regulation via a sacrificial template strategy and investigated the synergistic effects of hollow cavity and multi-magnetic components on the EM wave absorption.

Just Accepted

Benefiting from the cooperative merits of matched impedance, enhanced conduction loss, promoted interfacial polarization and strong magnetic loss, hollow CoNi microspheres display a maximum reflection loss of -62.9 dB and wideband absorption of 7.5 GHz with 15 wt% filler loading. More importantly, the microspheres realize prominent specific reflection loss and specific effective absorption bandwidth than the vast majority of counterparts.

2. Experimental sections

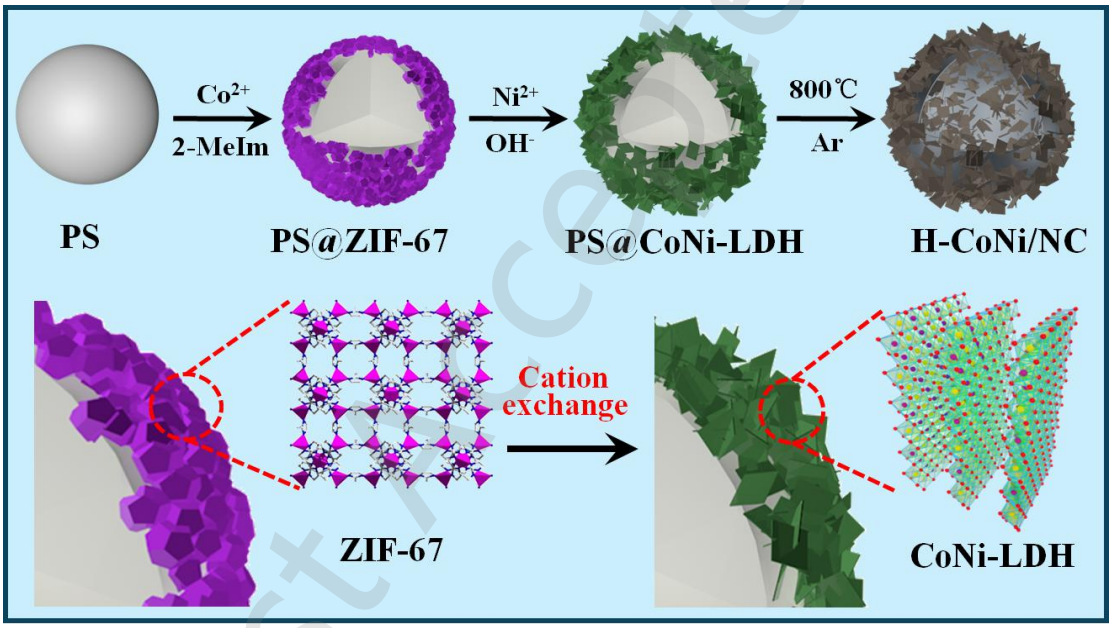

Figure 1. Schematic illustration for the synthetic process of H-CoNi@NC.

The synthetic process of hollow CoNi microspheres is shown in Figure 1. First, ZIF-67 polyhedrons are assembled on pre-prepared PS microspheres surface to form core-shell PS@ZIF-67 microspheres. Second, core-shell PS@ZIF-67 microspheres are transformed into core-shell PS@CoNi-LDHs microspheres via the cation exchange reaction. Third, hollow CoNi/N-doped carbon (H-CoNi/NC) microspheres are obtained after a pyrolysis process. For comparison, hollow Co/N-doped carbon (H-Co/NC) microspheres and solid CoNi/N-doped carbon (S-CoNi/NC) polyhedrons

Just Accepted

are obtained, respectively. The detailed information of the synthetic process and the characterizations are shown in Supplementary Material.

3. Results and discussions

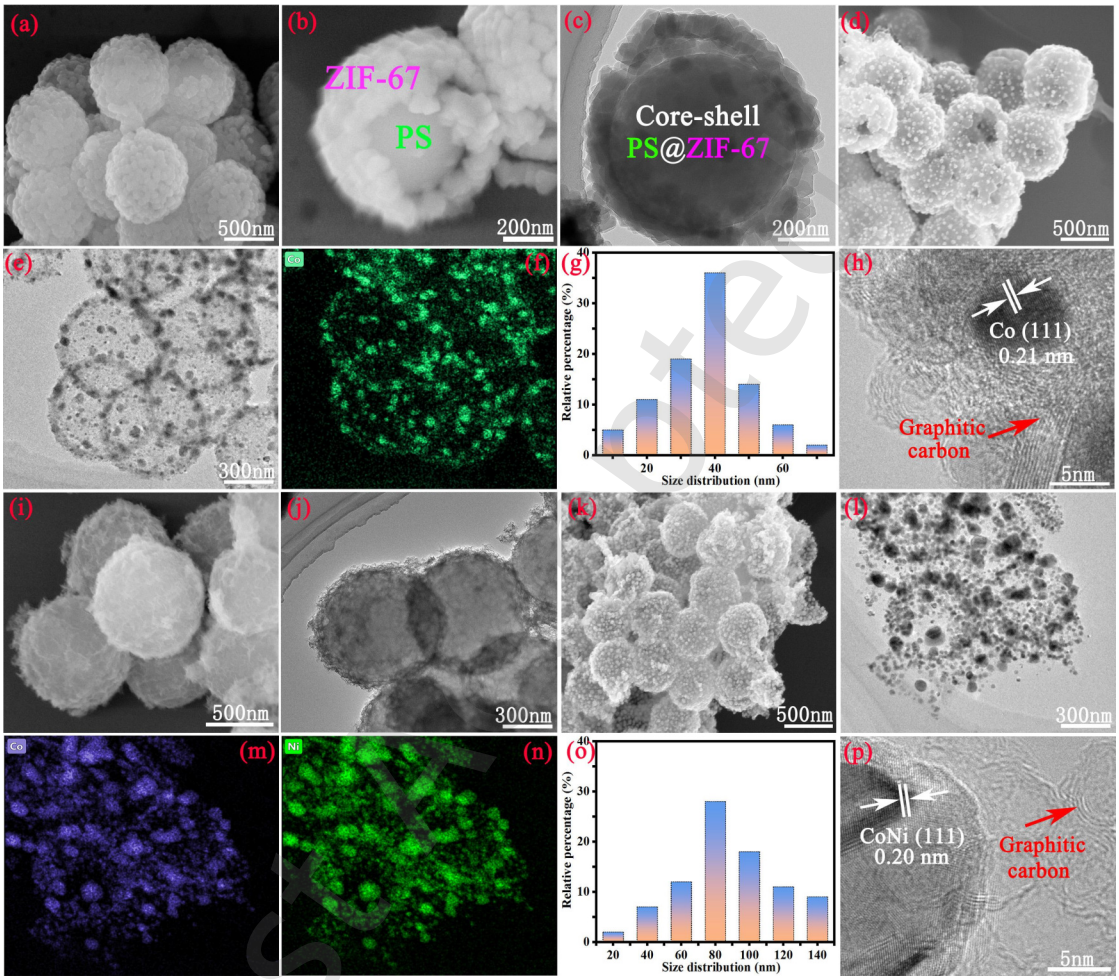

Figure 2. SEM images, TEM images, HRTEM images, the corresponding element mappings and Co size distribution of core-shell PS@ZIF-67 (a-c), H-Co/NC (d-h), core-shell PS@CoNi-LDHs (i,j) and H-CoNi/NC (k-p).

The morphologies and microstructures of core-shell PS@ZIF-67 microspheres, core-shell PS@CoNi-LDHs microspheres and their corresponding derivatives are shown in Figure 2. Typically, PS microspheres are obtained via a polymerization process. After that, assembled ZIF-67 polyhedrons are anchored on these pre-prepared

PS microspheres surface to form core-shell PS@ZIF-67 microspheres by mixing PS microspheres with mixed Co^{2+}/2-MeIm solution (Figure 2a-c). The element mappings reveal that C element mainly distributes in the inner region while Co/N elements mostly distribute in the outer region (Figure S1), confirming the successful generation of core-shell PS@ZIF-67 microspheres. After the pyrolysis process, outer ZIF-67 polyhedrons are converted into Co/NC particles (Figure 2d) and inner PS microspheres are completely carbonized to form hollow cavity (Figure 2e), resulting in the formation of H-Co/NC. Because of the strong coordination ability between Co^{2+} and 2-MeIm, the accumulative trend of reduced Co atoms is restricted to some extent, leading to the formation of small Co particles with an optimal size distribution of only 40 nm (Figure 2f,g). In Figure 2h, the presence of graphitic carbon layers is attributed to the catalytic effect of Co particles and the lattice spacing of 0.21 nm is indexed into the (111) plane of Co. After the cation exchange reaction, core-shell PS@ZIF-67 microspheres are transformed into core-shell PS@CoNi-LDHs microspheres. As presented in Figure 2i,j, SEM and TEM images show that these PS@CoNi-LDHs microspheres exhibit typically layered shapes, which are consistent with the results of the element mappings in Figure S2. As depicted in Figure S3, it is clear that the diffraction peaks at 11.6°, 22.8°, 33.8° and 60.1° are indexed to the (003), (006), (009) and (110) planes of CoNi-LDHs phase [34], and the disappeared diffraction peaks of ZIF-67 confirms the completely morphological transformation from ZIF-67 polyhedrons to CoNi-LDHs. After a pyrolysis process, core-shell PS@CoNi-LDHs microspheres are converted into H-CoNi/NC. In Figure 2k and Figure S4, it is distinct

Just Accepted

that these magnetic particles are tightly assembled to form hollow structure. In CoNi-LDHs, Co^{2+}/Ni^{2+} ions can move more freely during the carbonization/reduction process, thus generating large CoNi particles with an optimal size distribution of 80 nm, and the conclusions are confirmed by TEM and Co/Ni elemental mappings (Figure 2l-o), the lattice spacing of 0.20 nm is indexed into the (111) plane of CoNi alloys (Figure 2p). In order to emphasize the synergistic effects of morphological evolution and hollow engineering on the enhancement of impedance characteristics and EM wave absorption, S-CoNi/NC polyhedrons are prepared by directly annealing CoNi-MOF precursors (Figure S5), and the relevant analysis will be discussed in detail.

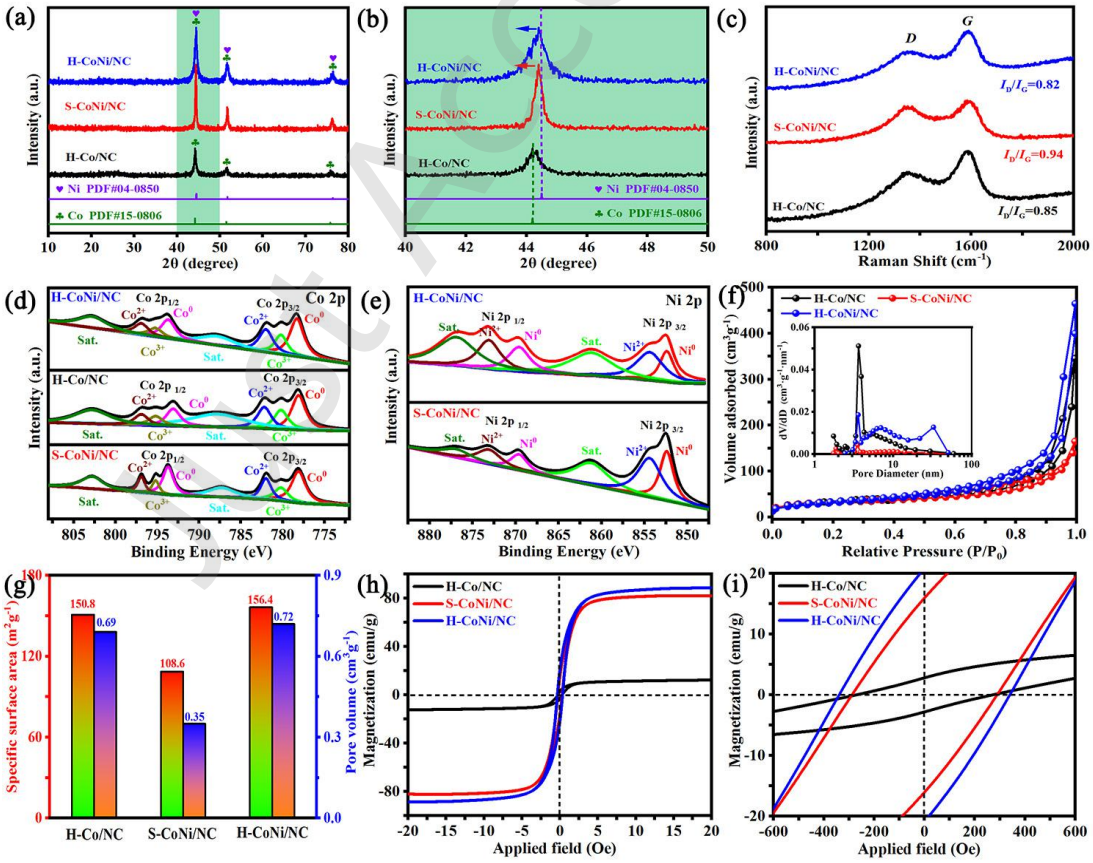

Figure 3. XRD pattern (a,b), Raman spectra (c), Co 2p (d), Ni 2p (e), N_2 absorption-desorption isotherms (f,g) and hysteresis loops (h,i) of H-Co/NC, S-CoNi/NC and H-CoNi/NC.

Not Accepted

The crystal structures of H-Co/NC, S-CoNi/NC and H-CoNi/NC are characterized by XRD pattern in Figure 3a. H-Co/NC exhibits three diffraction peaks at 44.2°, 51.5° and 75.8°, corresponding to the (111), (200) and (220) planes of metal Co (PDF#15-0806). As for S-CoNi/NC and H-CoNi/NC, the introduction of Ni species slightly shifts the diffraction peaks toward high angles (Figure 3b), suggesting a reduced lattice spacing, which is consistent with HRTEM images. In Figure 3c, Raman spectroscopy is conducted to evaluate the defect degree of carbon matrix. All samples display two characteristic peaks at 1350 cm^{-1} (D band) and 1580 cm^{-1} (G band), the former one corresponds to the structural disorder, while the later one represents the in-plane vibration of sp^2 carbon networks. Therefore, the I_D/I_G ratio can be identified to evaluate the defect degree. Clearly, the I_D/I_G ratios of H-Co/NC, S-CoNi/NC and H-CoNi/NC are 0.85, 0.94 and 0.82, respectively. The lowest ratio of H-CoNi/NC may be attributed to the fact that hollow engineering can significantly promote the catalytic effect for magnetic CoNi alloys. XPS is employed to analyze the chemical state of surface elements in Figure S6. It is obvious that the survey spectrums indicate the presence of C, N, O and Co elements, while the single of Ni element can be only detected in S-CoNi/NC and H-CoNi/NC. High resolution C1s spectrum (Figure S7) reveals that except for dominant C-C/C=C bonds, there are also some additional residual groups, such as C-N, C-O and C=O groups, which could act as polarized centers to induce dipolar loss [35]. As presented in Figure 3d for high resolution Co 2p spectrum, two peaks at 778.1 and 793.7 eV are ascribed to Co $2p_{3/2}$ and Co $2p_{1/2}$ of metallic Co^0, and the other peaks indicate the presence of partial

Just Accepted

oxidation states (Co^{2+} and Co^{3+}). As regard to high resolution Ni 2p spectrum (Figure 3e), the dominant characteristic peaks of metallic Ni^0 illustrate that Ni^0 species are completely doped in S-CoNi/NC and H-CoNi/NC to form CoNi alloys.

N_2 absorption-desorption isotherms are employed to analyze the specific surface and pore size distribution in Figure 3f. For H-Co/NC and H-CoNi/NC, the sharply increased trends of the hysteresis loops at high pressure suggest the presence of macropores owing to hollow engineering, and pore size analysis reveals that they possess optimal mesopores than that of S-CoNi/NC. Benefiting from the advantage of the co-existence of mesopores and macropores, the specific surface area and pore volume are 150.8 $m^2\ g^{-1}$ and 0.69 $cm^3\ g^{-1}$ for H-Co/NC, 156.4 $m^2\ g^{-1}$ and 0.72 $cm^3\ g^{-1}$ for H-CoNi/NC (Figure 3g), both of them are higher than that of S-CoNi/NC (108.6 $m^2\ g^{-1}$ and 0.35 $cm^3\ g^{-1}$). In general, high specific surface area and large pore volume could decrease the dielectric constant and adjust the impedance band gap between absorbents and air [36], resulting in matched impedance. The magnetic properties of H-Co/NC, S-CoNi/NC and H-CoNi/NC are characterized by VSM analysis at room temperature. As depicted in Figure 3h and Figure 3i, the saturation magnetization (M_s) and coercivity (H_c) values are 12.2 emu g^{-1} and 274.9 Oe for H-Co/NC, 81.9 emu g^{-1} and 293.4 Oe for S-CoNi/NC, 88.8 emu g^{-1} and 341.5 Oe for H-CoNi/NC, respectively. The significantly increased M_s for S-CoNi/NC and H-CoNi/NC is mainly attributed to the formation of CoNi alloys with both large size and strong magnetism, which is beneficial to the enhancement of magnetic loss and magnetic coupling [37]. Moreover, because of the morphological transformation from ZIF-67 to CoNi-LDHs,

Just Accepted

the derived H-CoNi/NC composites with high shape anisotropy display slightly larger H_c value than that of H-Co/NC and S-CoNi/NC.

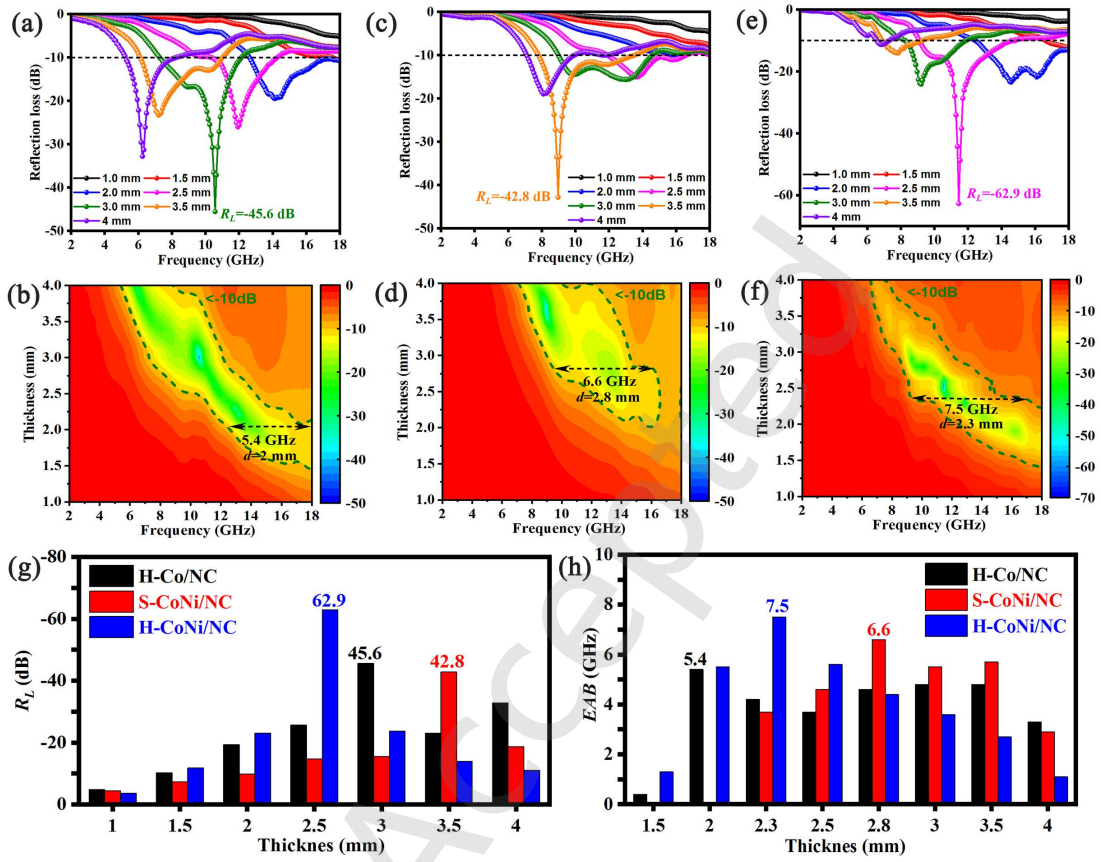

Figure 4. R_L values and 2D projection of H-Co/NC (a,b), S-CoNi/NC (c,d) and H-CoNi/NC (e,f), the comparation of R_L (g) and EAB (h) values for H-Co/NC, S-CoNi/NC and H-CoNi/NC.

The EM wave attenuation capability of all absorbents is evaluated based on transmission line theory with 15 wt% filler loadings. It is obvious that both the reflection loss (R_L) and effective absorption bandwidth (EAB, R_L≤-10 dB) closely correlate with the frequency and the corresponding thickness. As shown in Figure 4a, H-Co/NC displays a maximum R_L of -45.6 dB at a relatively lower matching thickness of 3 mm because compared with solid structure, hollow engineering can establish more conductive pathways by physical contacts to facilitate electron migration and hopping [38,39], therefore resulting in enhanced conduction loss.

Just Accepted

However, the insufficient magnetic loss can hardly optimize the impedance matching and promote absorption bandwidth. Therefore, the EAB is 5.4 GHz at 2.0 mm (Figure 4b). For S-CoNi/NC with multi-magnetic components, although the absorption intensity with a maximum R_L of -42.8 dB is weaker than H-Co/NC (Figure 4c), high saturation magnetization can broaden the absorption bandwidth and the EAB increases to 6.6 GHz at 2.8 mm (Figure 4d). From the above mentioned results, we can speculate that hollow engineering is benificial to the enhancement of absorption intensity while multi-magnetic components could broaden the absorption bandwidth [40]. Herein, H-CoNi/NC with both hollow cavity and multi-magnetic components is obtained via the morphological evolution after the cation exchange reaction, which could simultaneously exhibit high absorption intensity and wide absorption bandwidth. As expected in Figure 4e, the maximum R_L of H-CoNi/NC is up to -62.9 dB at 2.5 mm, and the EAB reaches as wide as 7.5 GHz at 2.3 mm (Figure 4f). Both the maximum absorption intensity and effective absorption bandwidth are higher than that of H-Co/NC and S-CoNi/NC in the measured thickness of 1-4 mm (Figure 4g,h), illustrating that the EM wave attenuation capability can be adjusted by hollow engineering and composition regulation [41].

Just Accepted

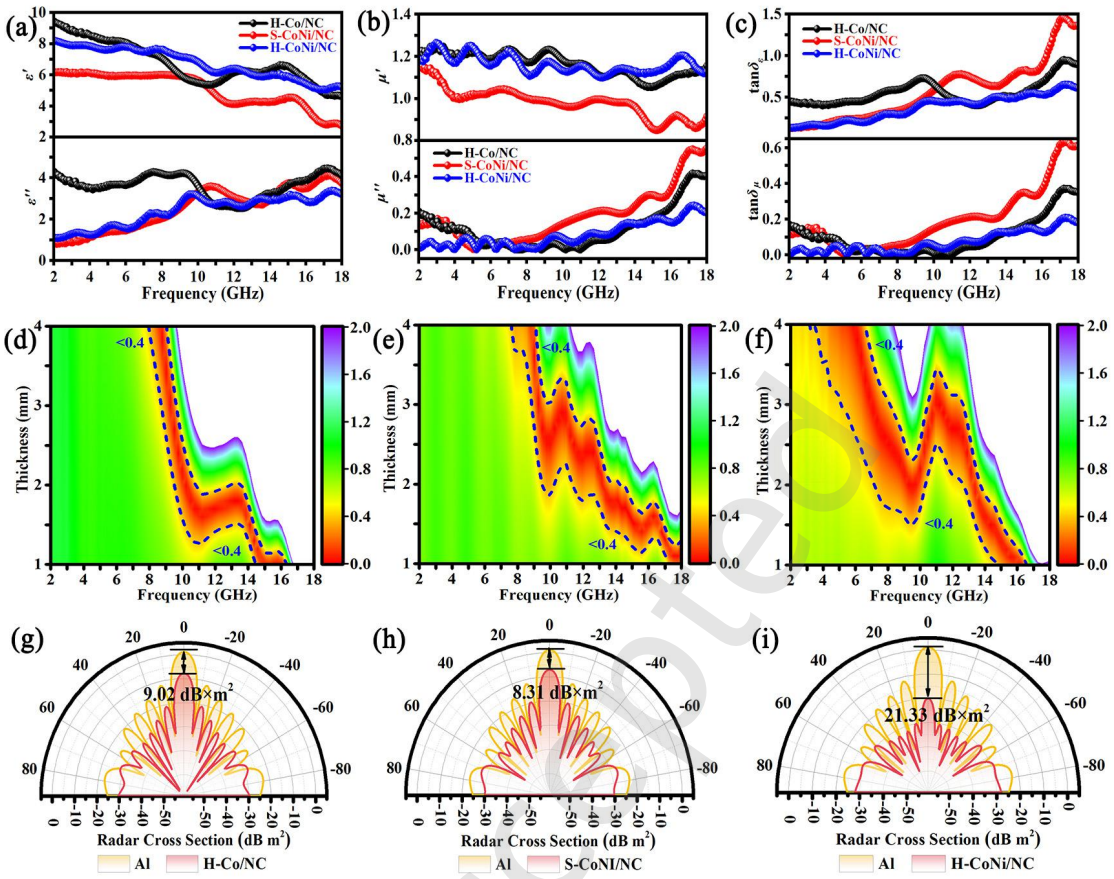

Figure 5. The relative complex permittivity (a), the relative complex permeability (b), tangent loss (c), $|Z_{in}/Z_0|$ values (d-f) and RCS curves (g-i) of H-Co/NC, S-CoNi/NC and H-CoNi/NC.

The EM parameters of H-Co/NC, S-CoNi/NC and H-CoNi/NC are measured to evaluate the EM wave attenuation behavior in Figure 5. As presented in Figure 5a, the ε' values gradually decrease with increasing the frequency, demonstrating the typical dielectric dispersion behavior [42,43]. Besides, the ε' values of H-Co/NC and H-CoNi/NC with hollow canvity are higher than that of S-CoNi/NC, resulting in enhanced conduction loss. As respect for S-CoNi/NC and H-CoNi/NC with multi-magnetic components, charge seperation occurs at the abundant heterogeneous interfaces, generating multiple interfacial polarization and dielectric relaxation under an alternating EM field [44], and resulting in increased ε'' values from 2 GHz to 18

Just Accepted

GHz. As shown in Figure 5b, S-CoNi/NC and H-CoNi/NC possess higher μ' and μ'' values than H-Co/NC in most frequency range, which is mainly attributed to the strong saturation magnetization of magnetic CoNi alloys. Moreover, it is obvious that the dielectric loss tangent ($\tan\delta_\varepsilon=\varepsilon''/\varepsilon'$) is higher than that of dielectric loss tangent ($\tan\delta_\mu=\mu''/\mu'$) for all absorbents in Figure 5c, confirming the dominant nature of dielectirc loss mechanism. Herein, the precondition of matching characteristics is evaluated by a delta-function method (Δ), which intuitively reflects the intrinsic impedance between absorbents and free space. In general, the Δ value less than 0.4 usually mean matched impedance. As dipected in Figure 5d-f, the strip area below 0.4 for H-CoNi/NC is larger than H-Co/NC and S-CoNi/NC, demonstrating the promoted impedance matching, and the optimized characteristics mainly originates from the cooperative effects of hollow engineering and composition regulation, in which the former one could significantly decrease the dielectric constant by introducing cavity and the later one could greatly induce strong magnetic loss by forming CoNi alloys [45,46]. In Figure 5g-i, radar cross-section (RCS) simulations are constructed to illustrate the practical applications under different incident angles. It is clear that all coatings covered on pure Al plates display decreased RCS values, confirming the strong ability to reduce radar detectability [47]. Typically, the RCS reduction values of H-CoNi/NC are higher than H-Co/NC and S-CoNi/NC in $-90°<\theta<90°$, and the highest RCS reduction value is 21.33 dB m^2 when the incident angle is 0°, suggesting the superior EM wave dissipation capacity for H-CoNi/NC.

To further clarify the relaxation mechanism associated with dielectric loss,

Just Accepted

Cole-Cole semicircles of H-Co/NC, S-CoNi/NC and H-CoNi/NC are analyzed in Figure S8. According to the Debye relaxation theory, each semicircular arc represents an individual Debye relaxation process [48]. Clearly, S-CoNi/NC and H-CoNi/NC display more Cole-Cole semicircles than H-Co/NC, indicating enhanced interfacial polarization [49]. The results demonstrate the construction of multi-magnetic components with hetero-interfaces significantly promotes polarization relaxation [50,51]. Moreover, some Cole-Cole semicircles are distorted and the curves in H-CoNi/NC become small, illustrating interfacial polarization makes a non-negligible effect in polarization relaxation [52]. Except for dielectric loss, magnetic loss also plays a crucial role in regulating impedance characteristic and promoting absorption performance. As shown in Figure 6a, it is distinct that the $\mu''(\mu')^{-2}f^{1}$ values almost keep unchanged in 4-18 GHz, suggesting that ferromagnetic resonance and eddy current loss simultaneously contribute to magnetic loss [53]. In particular, the attenuation constant (α) is employed according to the following equation [54,55]:

$$\alpha = \frac{\sqrt{2}\pi f}{c}\sqrt{(\mu''\varepsilon'' - \mu'\varepsilon') + \sqrt{(\mu''\varepsilon'' - \mu'\varepsilon')^2 + (\mu'\varepsilon'' + \mu''\varepsilon')^2}} \qquad (1)$$

Benefiting from the enhanced conduction loss caused by established conductive networks, promoted polarization relaxation induced by multiple hetero-interfaces and strong magnetic loss triggered by multi-magnetic components (Figure 6b), the H-CoNi/NC microspheres display higher attenuation constant than H-Co/NC and S-CoNi/NC in the measured frequency range (Figure 6c), demonstrating the superior EM wave attenuation capability [56-58]. To evaluate the EM attenuation capability for practical applications, the specific reflection loss (SRL, SRL=$|R_L|$/(filler

Just Accepted

loading×thickness)) and specific effective absorption bandwidth (SEAB, SEAB=EAB/(filler loading×thickness)) are calculated. Compared with the vast majority of reported absorbents (Figure 6d), the optimized H-CoNi/NC microspheres exhibit both superior SRL and SEAB values, demonstrating the efficient EM wave absorption performance.

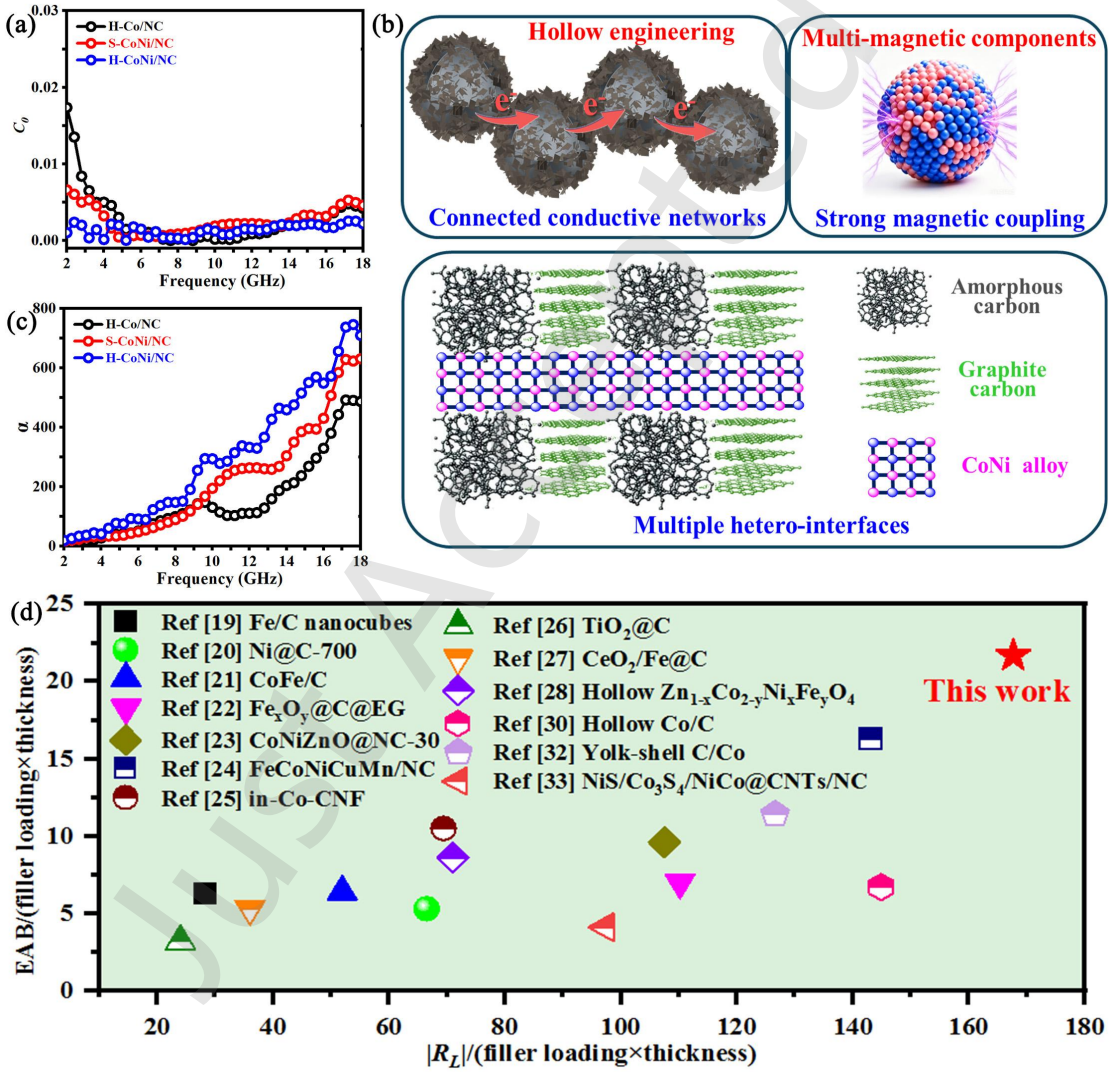

Figure 6. The C_0 values (a), the intrinsic absorption mechanism (b) and the α values of H-Co/NC, S-CoNi/NC and H-CoNi/NC, the SRL_{lt}/$SEAB_{lt}$ values of H-CoNi/NC compared with other MOF derived absorbents (d).

4. Conclusions

In summary, we have successfully synthesized hollow CoNi microspheres with multi-magnetic components via a sacrificial template strategy. Results indicate that the sacrificial template displays a dominant role in constructing hollow cavity and the morphological evolution plays an indispensable role in regulating the magnetic components. Benefiting form the cooperative merits of matched impedance matching, enhanced conduction loss, multiple interfacial polarization and strong magnetic loss, the obtained H-CoNi/NC microspheres display a maximum reflection loss of -62.9 dB at 2.5 mm and a broad bandwidth of 7.5 GHz at 2.3 mm with 15 wt% filler loading, demonstrating superior specific reflection loss and specific effective absorption bandwidth than most of the counterparts.

Just Accepted

Acknowledgments

This work was financially supported by National Natural Science Foundation of China (22308283, 52373271), Key Research and Development Project of Shaanxi Province (2025CY-YBXM-150). The authors acknowledge the support given by the Youth Innovation Team of Shaanxi Universities. The authors extend their gratitude to Sun Menghan (from Scientific Compass www.shiyanjia.com) for providing invaluable assistance with the VSM analysis.

References

[1] Cheng, S. Y.; Chen, Z. L.; Sheng, D. H.; Dong, W.; Cao, R.; Su, Z. B.; Wu, M. D.; Zhu, X. F.; Xie, A. M.; Mukherjee, S.; Li, W. J. Sustainable electromagnetic interference shielding materials from cellulose-grafted n-type polymers. *Nat. Commun.* **2025**, *16*, 8608.

[2] Zhang, Y. L.; Ruan, K. P.; Zhou, K.; Gu, J. W. Controlled distributed $Ti_3C_2T_x$ hollow microspheres on thermally conductive polyimide composite films for excellent electromagnetic interference shielding. *Adv. Mater.* **2023**, *35*, 2211642.

[3] Fan, X. X.; Zhang, X. C.; Li, L.; Cao, M. S. Recent progress and perspective of microwave absorption materials derived from metal organic frameworks. *Soft Sci.* **2024**, *4*, 43.

[4] Liu, X. Y.; Zhao, Y.; Zhang, Y. L.; Cui, X. C.; Xue, Y.; Lu, X. Y.; Gu, J. W. Bioinspired layered-gradient nanocomposites for intelligent electromagnetic skins with GHz-THz wave absorption, shielding, and solvent-driven actuation. *Nano-Micro Lett.* **2026**, *18*, 344.

[5] Chen, Q. Q.; Ma, Q. J.; Hu, Z. Y.; Zhang, J. Y.; Lin, C. Y.; Ge, J.; Bi, S.; Hou, Z. L. Breaking permittivity-loss constraint via surface and bulk carrier engineering in topological insulator Bi_2Te_3. *Adv. Funct. Mater.* **2026**, *36*, e18771.

[6] Qi, J. M.; Liang, C. B.; Ruan, K. P.; Li, M. K.; Guo, H.; He, M. K.; Qiu, H.; Guo, Y. Q.; Gu, J. W. Cactus-like architecture for synergistic microwave absorption and thermal management. *Nat. Sci. Rev.* **2025**, *12*, nwaf394.

[7] Cai, B.; Zhou, L.; Zhao, P. Y.; Peng, H. L.; Hou, Z. L.; Hu, P. F.; Liu, L. M.; Wang, G. S. Interface-induced dual-pinning mechanism enhances low-frequency electromagnetic wave loss. *Nat. Commun.* **2024**, *15*, 3299.

[8] Wang J. E.; Ming, W.; Chen, L.F.; Song, T. L.; Yele, M. X.; Zhang, H.; Yang, L.; Sarula, G.; Liang, B. L.; Yan, L. T.; Wang, G. S. MoS_2 lubricate-toughened MXene/ANF composites for multifunctional electromagnetic interference shielding.

Just Accepted

Nano-Micro Lett. **2025**, *17*, 36.

[9] Han, Y. X.; Yang, Y. R.; Li, T. H.; Zhang, Y. L.; Guo, H.; He, M. K.; Han, K. H.; Qiu, H.; Gu, J. W. Hierarchical heterogeneous Co-based magnetic absorbers for superior broadband high-efficiency microwave absorption. *Adv. Funct. Mater.* **2026**, *36*, e25719.

[10] Wang, H. Y.; Sun, X. B.; Yang, S. H.; Zhao, P. Y.; Zhang, X. J.; Wang, G. S.; Huang, Y. 3D Ultralight hollow NiCo compound@MXene composites for tunable and high-efficient microwave absorption. *Nano-Micro Lett.* **2021**, *13*, 206.

[11] Zhao, L.; Qian, Y. X.; Xu, X. F.; Wan, G. P.; Yu, L.; Yan, Y. Z.; Zhao, J. C.; Wu, L. H.; Dou, Z. F.; Wang, G. Z. Thermal-insulating carbon foam for efficient electromagnetic energy absorption and conversion. *Nano Energy* **2025**, *143*, 111313.

[12] Meng, Y. T.; Cai, B.; Zhou, Y. T.; Zhou, L.; Zhang, Y.; Wang, J. H.; Sarula, G.; Yan, L. T.; Lu, M.; Liang, B. L.; Wang, G. S. Bionic coral reef inspired enhanced scattering of trimetallic LDH self-assembled $Ti_3C_2T_x$ MXene for advanced microwave absorption. *Nano Res.* **2025**, *18*, 94907842.

[13] Ding, H.; Sun, Z. H.; Tian, S. Y.; Zhao, L. L.; Qian, L. Engineering the $CoSe_2$ phase transition in a Br-induced confined space for high-performance electromagnetic wave absorption. *J. Mater. Chem. A* **2025**, *13*, 12300-12312.

[14] Liu, P. B.; Zhang, G. Z.; Xu, H. X.; Cheng, S. C.; Huang, Y.; Ouyang, B.; Qian, Y. T.; Zhang, R. X.; Che, R. C. Synergistic dielectric-magnetic enhancement via phase-evolution engineering and dynamic magnetic resonance. *Adv. Funct. Mater.* **2023**, *33*, 2211298.

Just Accepted

[15] Liang, J.; Zhu, S. Y.; Chen, D. W.; Li, Y. J.; Zhou, D.; Meng, N.; Liao, Y. Z.; Sun, H. X.; Kong, J. Dual built-in electric field engineering in heterostructure nickel-cobalt bimetallic composites for boosted electromagnetic energy dissipation. *Adv. Powder Mater.* **2025**, *4*, 100344.

[16] Gao, Z. G.; Iqbal, A.; Hassan, T.; Hui, S. C.; Wu, H. J.; Koo, C. M. Tailoring built-in electric field in a self-assembled zeolitic imidazolate framework/MXene nanocomposites for microwave absorption. *Adv. Mater.* **2024**, *36*, 2311411.

[17] Zhang, S. J.; Zheng, J. J.; Zhao, Z. W.; Du, S. X.; Lan, D.; Gao, Z. G.; Wu, G. L. New prospects in built-in electric fields for electromagnetic wave absorption: from fundamentals to interdisciplinary applications. *Adv. Funct. Mater.* **2026**, *36*, e13762.

[18] Guo, Z. Y.; Qin, L. Y.; Zhang, Z.; Guan, Y. D.; Yang, Y.; Jiang, W.; Liu, R. B.; Shu, Q. H.; Zhou, J. D. Built-in electric fields in FeTe@expanded graphite heterostructures for enhanced electromagnetic wave absorption. *Nano Res.* **2025**, *18*, 94908109.

[19] Qiang, Q.; Du, Y. C.; Zhao, H.; Wang, Y.; Tian, C.; Li, Z.; Han, X. J.; Xu, P. Metal organic framework-derived Fe/C nanocubes toward efficient microwave absorption. *J. Mater. Chem. A* **2015**, *3*, 13426-13434.

[20] Liu, D. W.; Du, Y. C.; Xu, P.; Liu, N.; Wang, Y. H.; Zhao, H. H.; Cui, L. R.; Han, X. J. Waxberry-like hierarchical Ni@C microspheres with high-performance microwave absorption. *J. Mater. Chem. C* **2019**, *7*, 5037-5046.

[21] Liang, X. H.; Wang, G. H.; Gu, W. H.; Ji, G. B. Prussian blue analogue derived carbon-based composites toward lightweight microwave absorption. *Carbon* **2021**,

Just Accepted

177, 97-106.

[22] Yang, H. W.; Qiu, S. B.; Wang, L.; Li, Q. Q.; Che, R. C. Heterogeneous interface engineering in Fe_xO_y@C@Expanded graphite array structure with confined magnetic coupling to boost microwave absorption. *Carbon* **2025**, *242*, 120434.

[23] Yan, J. T.; Bai, W. H.; Cui, C.; Jiang, S.; Wang, W. J.; Tang, H.; Guo, R. H. Metal-organic framework-derived lilac flower-like CoNiZnO@nitrogen-doped carbon composites via a trapping microwave strategy for efficient absorption. *J. Mater. Chem. A* **2024**, *12*, 28794-28804.

[24] Lv, F. Y.; Wang, Y. Q.; He, Q. C.; Lan, D.; Wu, G. L. High-entropy strategy-driven lattice distortion and electronic rearrangement in MOF-derived HEA/NC composites for balanced electromagnetic response and superior microwave attenuation. *Adv. Funct. Mater.* **2026**, e75416.

[25] Cao, X. H.; Wu, X. Y.; Wang, X.; Luo, J. M.; Zhang, Z.; Xue, Y.; Zhang, G. L.; Zhang, L. Y.; Zhang, H.; Yu, J. Y. Mechanistic insights into the structural evolution of ZIF-67 via electrospinning strategy toward high electromagnetic wave absorption performance of ZIF-67-derived carbon nanofibers. *Adv. Sci.* **2025**, *12*, 2502560.

[26] Zhou, L.; Shakil, M. I.; He, J. Y.; Zhang, X. Y.; Wang, H. B. MIL-125(Ti)-derived core-shell TiO_2@C composites for tunable and efficient microwave absorption. *Compos. Part B-Eng.* **2026**, *322*, 113764.

[27] Zhang, X.; Tai, H. B.; Wang, X. L.; Lu, J. Q.; Zheng, C. Y.; Liu, Z. L. MOF-on-MOF-derived CeO_2/Fe@C composites for tunable low-frequency electromagnetic wave absorption. *Small* **2026**, e73658.

Just Accepted

[28] Ding, L. F.; He, Z. Z.; Zhang, R. N.; Liu, S. H.; Geng, W. C.; Liu, P. B. Hollow $Zn_{1-x}Co_{2-y}Ni_xFe_yO_4$ spinel via multi-metal ion doping: ultralight and broadband microwave absorber. *Soft Sci.* **2026**, *6*, 2.

[29] Lv, Z. R.; Liu, M. C.; Yang, Y.; Chen, T. H.; Yang, W. Y.; Wang, Y. J.; Zhao, Z. W.; Lan, K.; Zhao, T. C.; Li, Q. W.; Li, X. M.; Zhao, D. Y. Hierarchical engineering of single-crystalline mesoporous metal-organic frameworks with hollow structures. *J. Am. Chem. Soc.* **2025**, *147*, 14585-14594.

[30] Li, Z. N.; Han, X. J.; Ma, Y.; Liu, D. W.; Wang, Y. H.; Xu, P.; Li, C. L.; Du, Y. C. MOFs-derived hollow Co/C microspheres with enhanced microwave absorption performance. *ACS Sustainable Chem. Eng.* **2018**, *6*, 8904-8913.

[31] Liu, P. B.; Gao, S.; Zhang, G. Z.; Huang, Y.; You, W. B.; Che, R. C. Hollow engineering to Co@N-doped carbon nanocages via synergistic protecting-etching strategy for ultrahigh microwave absorption. *Adv. Funct. Mater.* **2021**, *31*, 2102812.

[32] Zhou, J. T.; Zou, K. X.; Tao, J. Q. Liu, J.; Liu, Y. J.; Duan, L. T.; Cheng, Z. Y.; Zha, B. R.; Yao, Z. J.; Peng, G. Y.; Tao, X. W.; Huang, H. X.; Ma, Y.; Liu, P. J. Using multi-scale interaction mechanisms in yolk-shell structured C/Co composite materials for electromagnetic wave absorption. *J. Mater. Sci. Technol.* **2025**, *215*, 36-44.

[33] Chen, Y. K.; Wang, X. Q.; Cui, W. G.; Gao, Y.; Pan, H. G.; Wang, Y.; Che, R. C. Multiple schottky contacts motivated via defects to tune the response ability of wlectromagnetic waves. *Adv. Funct. Mater.* **2025**, *35*, 2417215.

[34] Li, D.; Gan, R. H.; Zheng, Y. P.; Chen, C.; Wan, J. W. Unraveling the role of Co-O-Ni motifs in MOF-derived CoNi-LDH for enhanced oxygen evolution reaction.

Just Accepted

Chem. Commun. **2026**, *62*, 5970-5974.

[35] Han, Y. X.; He, M. K.; Hu, J. W.; Liu, P. B.; Liu, Z.; Ma, Z.; Ju, W. B.; Gu, J. W. Hierarchical design of FeCo-based microchains for enhanced microwave absorption in C band. *Nano Res.* **2023**, *16*, 1773-1778.

[36] Liu, X.; Qian, Y. X.; Yu, L.; Si, Z. K.; Wu, L. H.; Wan, G. P.; Xu, X. F.; Wang, G. Z. Regulating local coordination environment of single-atom Co absorbers for dielectric-magnetic dual loss modulation. *Adv. Mater.* **2026**, *38*, e72966.

[37] He, M. K.; Hu, J. W.; Yan, H.; Zhong, X.; Zhang, Y. L.; Liu, P. B.; Kong, J.; Gu, J. W. Shape anisotropic chain-like CoNi/polydimethylsiloxane composite films with excellent low-frequency microwave absorption and high thermal conductivity. *Adv. Funct. Mater.* **2025**, *35*, 2316691.

[38] Wu, R. Q.; Sun, Y. J.; Jiang, X. Z.; Yu, H. Y.; Flower-like multi-shell hollow microsphere enhances dielectric-magnetic synergy for efficient microwave absorption in C- band. *ACS Appl. Mater. Interfaces* **2026**, *18*, 8622-8635.

[39] Wen, L. C.; Cheng, S. Y.; Shang, H. C.; Sheng, D. H.; Li, W. J.; Qi, X. S.; Xie, A. M. Regulating interfacial strain from tensile to compressive state in transition-metal-sulfides/carbon for high-performance electromagnetic wave absorption. *Adv. Funct. Mater.* **2026**, *36*, e74621.

[40] Liu, A.; Xu, X. S.; Qiu, H.; Guo, H.; He, M. K.; Yu, Z.; Zhang, Y. L.; Gu, J. W. Bioinspired hollow heterostructure fillers for enhanced electromagnetic interference shielding in polyimide aerogels. *InfoMat* **2025**, *7*, e70060.

[41] He, M. K.; Zhong, X.; Lu, X. H.; Hu, J. W.; Ruan, K. P.; Guo, H.; Zhang, Y. L.;

Just Accepted

Guo, Y. Q.; Gu, J. W. Excellent low-frequency microwave absorption and high thermal conductivity in polydimethylsiloxane composites endowed by hydrangea-like CoNi@BN heterostructure fillers. *Adv. Mater.* **2024**, *36*, 2410186.

[42] Peng, H. L.; Cai, B.; Zhang, Y.; Gao, L. C.; Zhao, P. Y.; Zhou, L.; Zhang, S.; Liang, W. H.; Xuan, Q. F.; Koo, M. C.; Liang, C. M.; Li, W. P.; Hou, Z. L.; Zhou, T.; Wang, G. S. Radar-terahertz-infrared compatible stealth coaxial silver nanowire@carbon nano-cable aerogel. *Angew. Chem. Int. Ed.* **2025**, *64*, e202421090.

[43] He, M. K.; Gu, J. W. Tunable low-frequency microwave absorption and thermal management through in-situ confined growth of alloys within aramid nanofibers. *ENG. TM.* **2026**, DOI:10.2738/ENGTM.2026.0001.

[44] Sheng, D. H.; Cheng, S. Y.; Zhang, M. M.; Zhang, J. L.; Zhu, X. F.; Li, W. J.; Zhang, B.; Xie, A. M. Nanocurvature-activated dipolar polarization in M-N_4 single-atom sites for high-performance electromagnetic wave absorption. *Adv. Sci.* **2026**, *0*, e75115.

[45] Zhang, H.; Kuang, K. L.; Zhang, Y. F.; Sun, C.; Yuan, T. K.; Yin, R. L.; Fan, Z.; Che, R. C.; Pan, L. J. Multifunctional carbon foam with nanoscale chiral magnetic heterostructures for broadband microwave absorption in low frequency. *Nano-Micro Lett.* **2025**, *17*, 133.

[46] Gong, X. F.; Xiang, L. L.; Qi, X. S.; Gong, X.; Chen, Y. L.; Peng, Q.; Qu, Y. P.; Wu, F. Z.; Sun, K.; Zhong, W. Improved polarization loss and impedance matching induced by carbon paper-based magnetic heterostructured composites for lightweight and strong microwave absorption. *Adv. Compos. Hybrid Mater.* **2024**, *7*, 216.

Just Accepted

[47] Chen, N.; Han, B. B.; Li, J. F.; Hu, J. H.; Guan, Z. J.; Jiang, J. T.; Wang, K. J.; Pan, Y. T. Yolk-shell engineering on single-component Fe_3O_4 to realize magnetic-dielectric synergy for enhanced microwave absorption: experimental and simulation insights. *ACS Appl. Mater. Interfaces* **2026**, *18*, 17143-17155.

[48] Ming, W.; Yang, L.; Chen, H. X.; Fei, F.; Zhang, H.; Sarula, G.; Wang, J. H.; Wang, T. Y.; Jin, C. Z.; Liang, B. L.; Zhang, L.; Yan, L. T. High toughness MXene/ANF-CZIF67/ANF "magnetic-electric" Janus film for multifunctional low reflection electromagnetic interference shielding. *Nano Res.* **2025**, *18*, 94907621.

[49] Liang, C. M.; Hou, Z. L.; Koo, M. C.; Xu, F. F.; Bai, S.; Bai, Y. X.; Zhang, Y.; Cai, B.; Zhao, P. Y.; Wang, G. S. Modulating electromagnetic response through the regulation of built-in electric fields. *J. Mater. Sci. Technol.* **2026**, *248*, 126-134.

[50] Zhong, X.; He, M. K.; Zhang, C. Y.; Guo, Y. Q.; Hu, J. W.; Gu, J. W. Heterostructured BN@Co-C@C endowing polyester composites excellent thermal conductivity and microwave absorption at C band. *Adv. Funct. Mater.* **2024**, *34*, 2313544.

[51] Wang, J. E.; Song, T. L.; Ming, W.; Yele, M. X.; Chen, L. F.; Zhang, H.; Zhang, X. J.; Liang, B. L.; Wang, G. S. High MXene loading, nacre-inspired MXene/ANF electromagnetic interference shielding composite films with ultralong strain-to-failure and excellent Joule heating performance. *Nano Res.* **2024**, *17*, 2061-2069.

[52] Niu, H. H.; Li, Y. Y.; Jiang, X. W.; Xia, Y. D.; Wang, H. L.; Zhang, R.; Li, H. X.; Fan, B. B.; Zhou, Y. C. Construction of hydrangea-like core-shell SiO_2@$Ti_3C_2T_x$@CoNi microspheres for tunable electromagnetic wave absorber. *J.*

Just Accepted

Adv. Ceram. **2023**, *12*, 711-723.

[53] Hu, J. X.; Yan, W. R.; Huang, X. Y.; Yi, C.; Pan, F. Z.; Xiao, L.; Wang, J.; Wang, W. F.; Zhao, D.; Zeng, H. F.; Man, Q. K.; Wu, M.; Tan, G. G.; Chi, X. Curvature‐induced anisotropy drives broadband magnetic loss and ultra‐strong microwave absorption. *Adv. Funct. Mater.* **2026**, *36*, e31603.

[54] Liu, Z.; Xue, Y. H.; Meng, Y. T.; Liang B. L. Reduced-reflectance bionic e-skin with electromagnetic-environmental-sensing integration enabled by Ni-reconstructed liquid metal networks. *Adv. Funct. Mater.* **2026**, e76178.

[55] Wu, L. H.; Liu, J.; Liu, X.; Mou, P. P.; Lv, H. M.; Liu, R.; Wen, J. G.; Zhao, J. C.; Li, J. L.; Wang, G. Z. Microwave-absorbing foams with adjustable absorption frequency and structural coloration. *Nano Lett.* **2024**, *24*, 3369-3377.

[56] Yelea, M. X.; Sarulaa, G.; Yang, J.; Yang, L.; Zhang, H.; Chen, L. F.; Zhang, X. M.; Wang, J. H.; Wang, T. Y.; Jin, C. Z.; Liang, B. L.; Yan, L. T. Integrated structural-functional MXene-GNs/ANF flexible composite film with enhanced thermal conductivity and electromagnetic interference shielding performance. *J. Mater. Sci. Technol.* **2026**, *241*, 200-210.

[57] Wu, Q. Q.; Ma, Z. L.; Tao, Y.; Wang, C. Y.; Jin, Z. Y.; Wang, S. Y.; Gao, T. D.; Li, C.; Liu, P. B. Carbon nanofibers with small-sized Co nanoparticles and structural defects via a confined-coordination growth strategy toward electromagnetic wave absorption. *J. Adv. Ceram.* **2025**, *14*, 9221210.

[58] Zhang, X.; Tian, X. L.; Wu, N.; Zhao, S. Y.; Qin, Y. T.; Pan, F.; Yue, S. Y.; Ma, X. Y.; Qiao, J.; Xu, W.; Liu, W.; Liu, J. R.; Zhao, M. T.; Ostrikov, K.; Zeng, Z. H.

Just Accepted

Metal-organic frameworks with fine-tuned interlayer spacing for microwave absorption. *Sci. Adv.* **2024**, *10*, eadl6498.

Just Accepted

Electronic Supplementary Material

Multi-magnetic regulation of hollow CoNi microspheres via morphological evolution for ultrahigh electromagnetic wave absorption

Wenqi Song[1,*], Chunyang Lan[1], Zhaona Du[1], Chenyu Wang[2], Panbo Liu[2,*]

[1]Technological Institute of Materials & Energy Science (TIMES); Shaanxi Key Laboratory of Liquid Crystal Polymer Intelligent Display; Key Laboratory of Liquid Crystal Polymers based Flexible Display Technology in National Petroleum and Chemical Industry; School of Materials and New Energy, Xijing University, Xi'an 710123, China

[2]School of Chemistry and Chemical Engineering, Northwestern Polytechnical University, Xi'an 710129, China

*Address corresponding to Wenqi Song, songwenqi@xijing.edu.cn; Panbo Liu, liupanbo@nwpu.edu.cn.

Supporting information to https://doi.org/10.26599/NR.2026.94909011

Just Accepted

Experimental sections

Preparation of PS microspheres. 0.22 g of sodium dodecyl sulfate and 0.2 g of potassium persulfate were dissolved in a 250 mL double necked flask containing 140 mL mixed solvent (100 mL of ethanol and 40 mL of deionized water). Styrene was treated three times by 10% sodium hydroxide solution in a separating funnel with the aim to remove the polymerization inhibitor. Then 9 mL of styrene was added in the flask, heated the solution to 70℃ under nitrogen atmosphere and stirred rapidly for 24 h. After the polymerization reaction, 9 mL of styrene diluted with ethanol was added and the solution was stirred for another 8 h. Finally, the obtained PS microspheres were collected by centrifugation and dispersed in 20 mL of methanol.

Preparation of PS@ZIF-67 microspheres. 1 mL of PS microspheres mixed with $Co(NO_3)_26H_2O$ (20 mM) and 2-MeIm (80 mM) were dissolved into 10 mL of methanol, and the mixed solution was stirred for 24 h. The products of PS@ZIF-67 microspheres were obtained by centrifugation washed with methanol. Besides, ZIF-67 polyhedrons were obtained without adding PS microspheres.

Preparation of PS@CoNi-LDHs microspheres. The PS@CoNi-LDHs microspheres were synthesized through an ion-exchange reaction. Briefly, 0.1 g of PS@ZIF-67 microspheres were dissolved into 50 mL of ethanol, then 0.1 g of $Ni(NO_3)_26H_2O$ was added and the mixed solution was stirred and refluxed at 90℃ for 5 h. Finally, the obtained products were collected by centrifugation.

Preparation of Co/Zn-MOF polyhedrons. Briefly, 5 mmol of $Co(NO_3)_26H_2O$ and 5 mmol of $Ni(NO_3)_26H_2O$ were dissolved in 150 mL of methanol to form solution A. 40

Just Accepted

mmol of 2-MeIm was dissolved in 150 mL of methanol to form solution B. Then solution B was quickly poured into solution A and the mixed solution was vigorously stirred for 24 h. The products of ZIF-67 polyhedrons were obtained by centrifugation washed with methanol.

Preparation of hollow Co/N-doped carbon (H-Co/NC), solid CoNi/N-doped carbon (S-CoNi/NC) and hollow CoNi/N-doped carbon (H-CoNi/NC). The obtained PS@ZIF-67 microspheres, Co/Zn-MOF polyhedrons and PS@CoNi-LDHs microspheres were annealed at a tubular furnace at 800℃ for 2 h with a heating rate of 5℃/min, resulting in the formation of H-Co/NC, S-CoNi/NC and H-CoNi/NC, respectively.

Characterizations. The microstructures were characterized by field emission scanning electron microscope (FESEM, Quanta 600FEG) and field emission transmission electron microscope (FETEM, Tecnai F30 G^2). The crystal phases were characterized by X-ray powder diffraction (XRD; Bruker, D8-Advance X-ray Diffractometer) with Cu Kα radiation (λ=0.15406 nm). Raman spectroscopy was carried out by Alpha300R (WITec). The element valence and composition were recorded by X-ray photoelectron spectrometer (XPS, PHI 5000 Versa Probe). The electromagnetic parameters were analyzed using a HP8753D vector network analyzer in 2-18 GHz. The samples were dispersed in paraffin with only 15 wt% filler loading, and the product was pressed into a toroidal shape with an inner diameter of 3.0 mm and an outer diameter of 7.0 mm. The reflection loss is calculated according to the following equations:

Just Accepted

$$R_L(\mathrm{dB}) = 20\log\left|\frac{Z_{in} - Z_0}{Z_{in} + Z_0}\right| \qquad \text{(Equation S1)}$$

$$Z_{\mathrm{in}} = Z_0\sqrt{\mu_r / \varepsilon_r}\tanh[j(2\pi fd / c)\sqrt{\varepsilon_r\mu_r}] \qquad \text{(Equation S2)}$$

where Z_0 is the characteristic impedance of free space, Z_{in} is the normalized input impedance of absorber, ε_r and μ_r are the relative complex permittivity and permeability, d is the layer thickness, c is the speed of light in free space and f is the corresponding frequency.

Just Accepted

Results and discussions

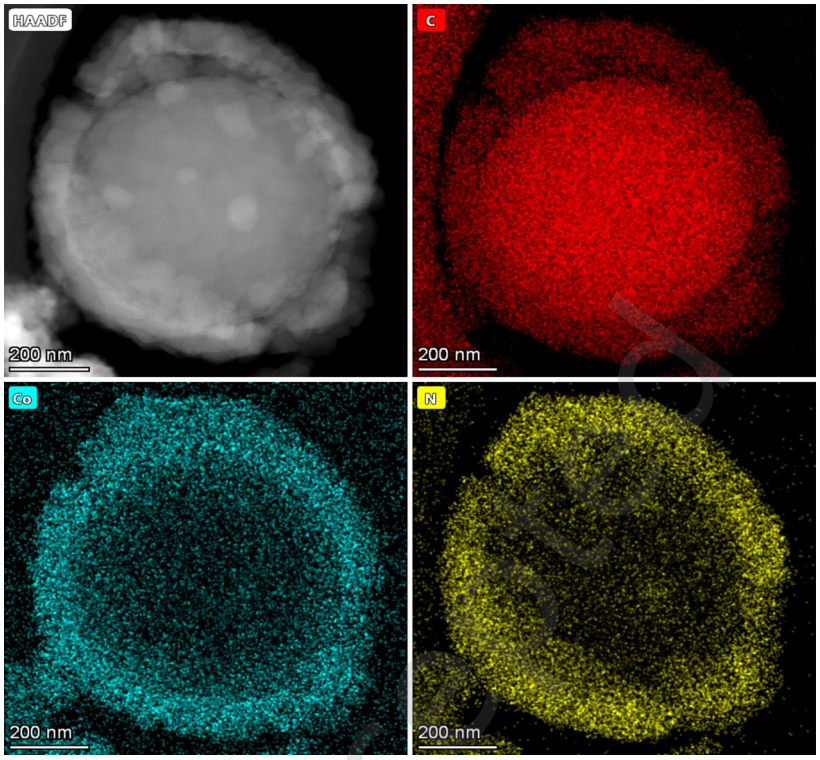

Figure S1. The element mappings of core-shell PS@ZIF-67 microspheres.

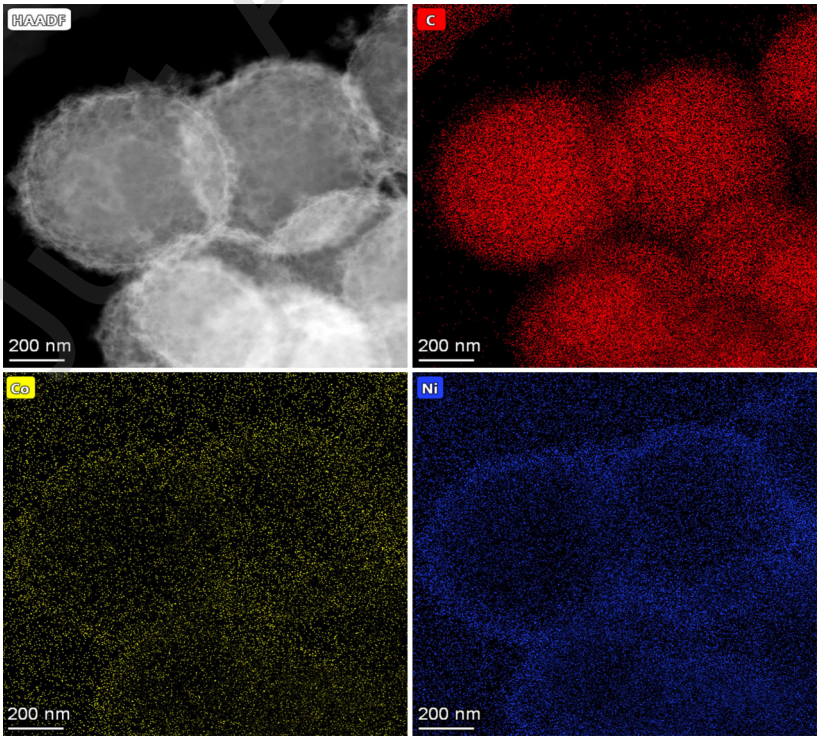

Figure S2. The element mappings of core-shell PS@CoNi-LDHs microspheres.

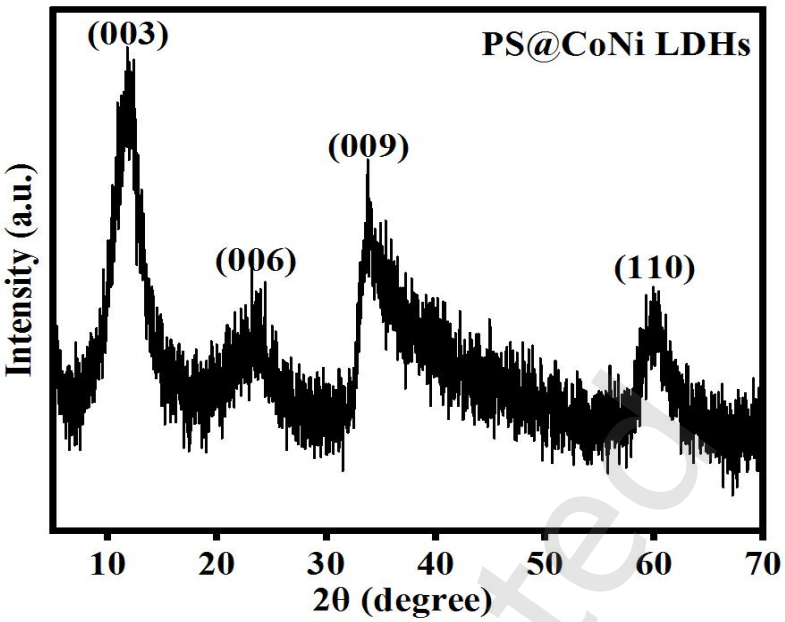

Figure S3. XRD pattern of core-shell PS@CoNi-LDHs microspheres.

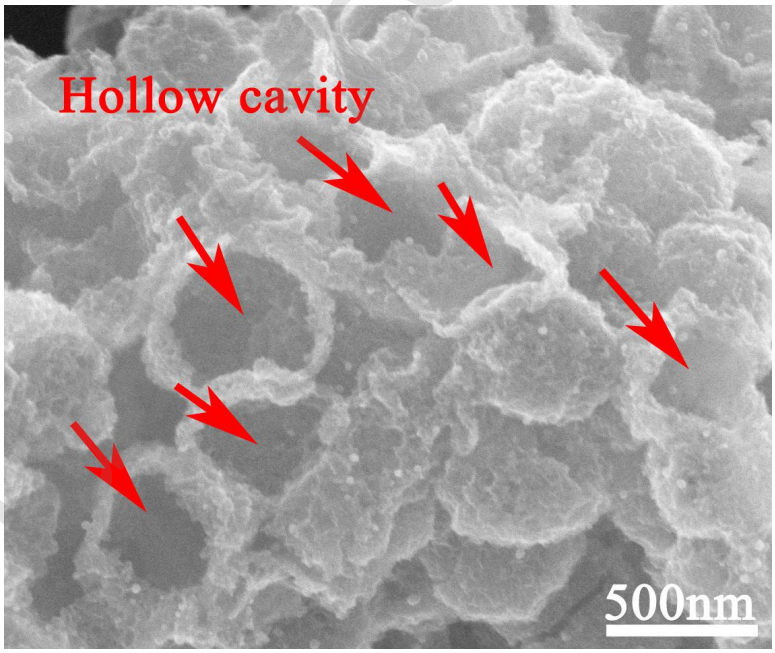

Figure S4. SEM image of H-CoNi/C.

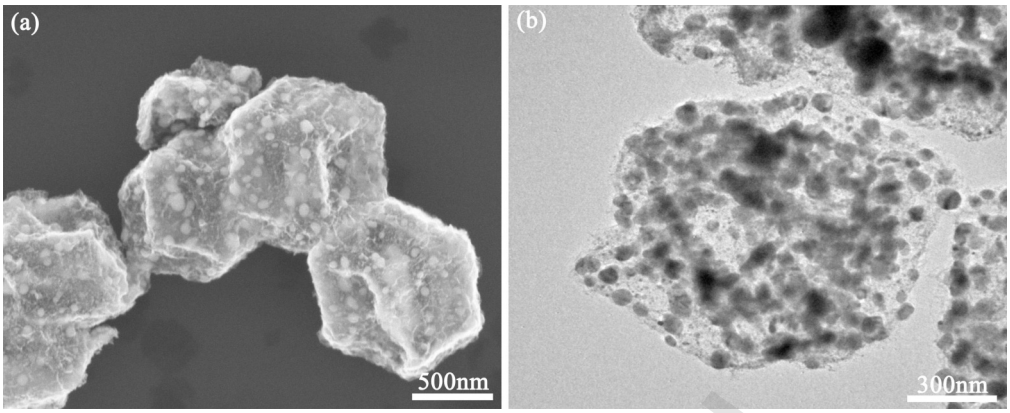

Figure S5. SEM and TEM image of S-CoNi/C.

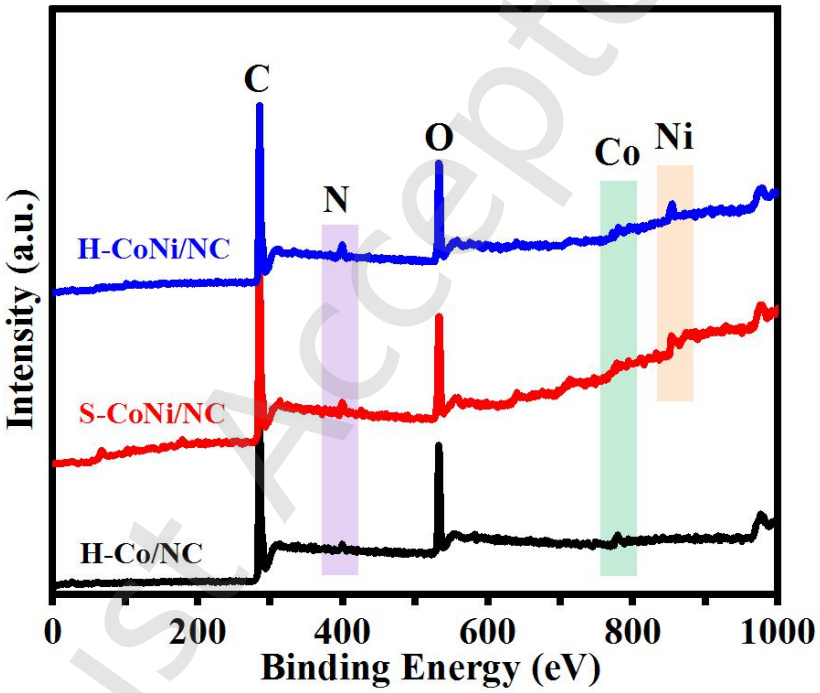

Figure S6. XPS survey spectra of H-Co/NC, S-CoNi/NC and H-CoNi/NC.

Just Accepted

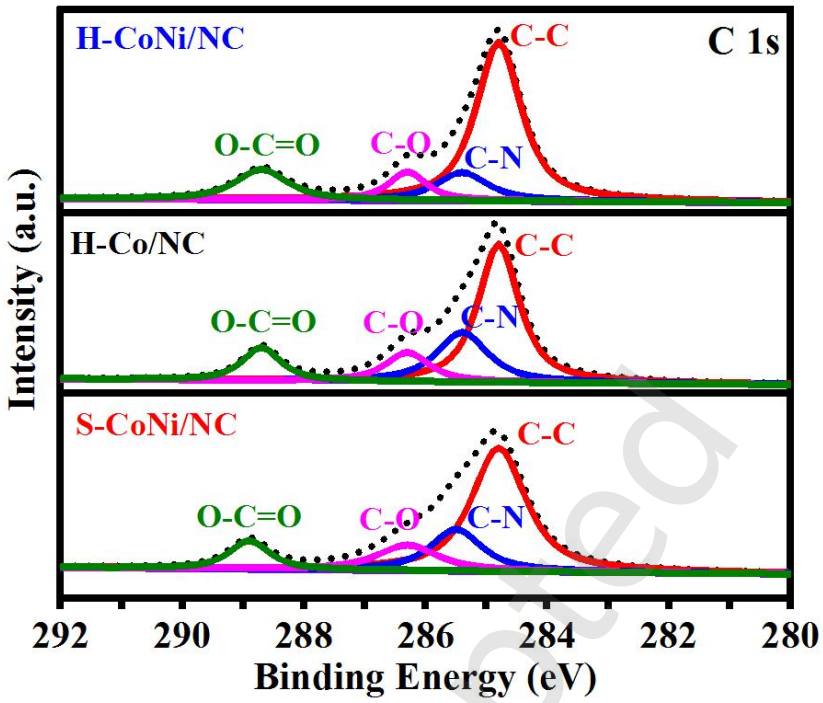

Figure S7. C 1s of H-Co/NC, S-CoNi/NC and H-CoNi/NC.

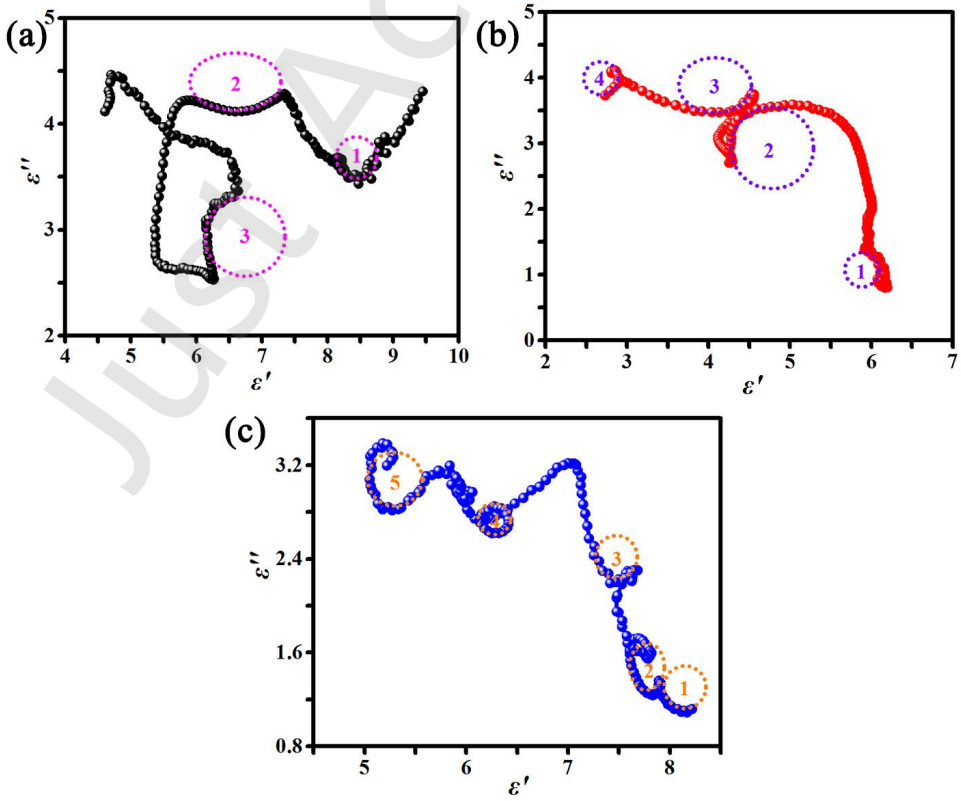

Figure S8. Cole-Cole curves of H-Co/NC (a), S-CoNi/NC (b) and H-CoNi/NC (c).

Just Accepted